AUT Journal of Modeling and Simulation

AUT J. Model. Simul., 49(2)(2017)143-152
DOI: 10.22060/miscj.2016.841

Thermo-Electro Mechanical Impedance based Structural Health Monitoring: Euler-Bernoulli Beam Modeling

N. Sepehry[1], F. Bakhtiari-Nejad[2*],M. Shamshirsaz[3]

[1] Faculty of Mechanical and Mechatronics Engineering, Shahrood University of Technology, Shahrood, Iran

[2] Dept. of Mechanical Engineering, Amirkabir University of Technology, Tehran, Iran

[3] New Technologies Research Center, Amirkabir University of Technology, Tehran, Iran

ABSTRACT: In recent years, impedance measurement method by piezoelectric (PZT) wafer active sensor (PWAS) has been widely adopted for non-destructive evaluation (NDE). In this method, the electrical impedance of a bonded PWAS is used to detect a structural defect. The electro-mechanical coupling of PZT materials constructs the original principle of this method. Accordingly, the electrical impedance of PWAS can sense any change in the mechanical impedance of the structure. A thermal stress on a structure, which was generated by environmental temperature, could change the electrical impedance of PWAS. The thermal stress which affects the output impedance of PWAS is also developed. A temperature-dependent model, the temperature dependency of PWAS, and structure material properties are investigated for a PWAS bonded to an Euler Bernoulli clamped-clamped beam. The Rayleigh-Ritz and spectral element methods are studied and, then, verified by 3D finite element method (FEM).

Review History:

Received: 9 December 2015
Revised: 13 February 2016
Accepted: 28 June 2016
Available Online: 12 November 2016

Keywords:
Thermal Stress
Euler Bernoulli Beam
Spectral Element Method
Impedance-based Structural Health Monitoring
3D FEM

1- Introduction

Impedance-based Structural Health Monitoring (ISHM) using PWAS as a sensor and an actuator have widely been investigated to find application in nondestructive evaluation (NDE) technique during the last few years [1-7]. Giurgiutiu and Rogers [1] presented a relation between electrical admittance (inverse of impedance) of a PWAS patch and structural mechanical impedance.

A high frequency voltage (in the order of kHz) applied to PWAS after it bound to the host structure. Because a small wavelength is needed to detect minor changes in the structure, this high-frequency method is appropriate for the detection of these types of changes. The size of impedance sensors used to directly measure the local dynamic response is small [2]. Because of the temperature dependency of PWAS and the structure's material properties, the impedance is affected by any change in the environmental temperature. Several studies investigated these effects [3-8]. A method based on the root mean square deviations (RMSD) to compensate the temperature effect has been proposed by Park et al. [5]. Bhalla et al. [3] proposed a temperature-dependent impedance model on a spring-mass-damper (SMD) system. The vertical and horizontal shift in PWAS impedance due to temperature variation was studied by Koo et al. [4]. Despite the importance of the issue, only the effect of temperature variation on PWAS and material properties of the structure were studied with theoretical investigation of transverse vibration modes for a cantilever Euler Bernoulli beam. Bastany et al. considered a sensor array and statistical metric analysis to compensate the environmental changes [6]. Also, a study proposed the combination of RMSD damage index and an artificial neural network based on RBF to compensate the temperature variation effect [7]. Few studies modeled the coupling effect of PWAS and base structures in ISHM [1, 8-14].

A model based on the mechanical impedances of a 2-D structure and PWAS was proposed by Bhalla and Soh [11]. Perairs et al. calculated the PWAS output electrical impedance using an equivalent electrical circuit for a Timoshenko beam [12]. A continuous model of a beam and PWAS for the calculation of the impedance of PWAS was developed by Giurgiutiu [9]. FEM is a time-domain method, which depends on polynomial functions, which are independent of frequency, for finding an approximate solution to a boundary value problem. Hence, FEM cannot be a proper method for high-frequency wave modes. Thus FEM, especially at high frequencies, is significantly inaccurate because wavelengths are very short [15]. The spectral element method (SEM) is one of the frequency-domain methods, used in high-frequency analyses. Several works have reported SEM for modeling beams and plates [15].

In this paper, a new model with consideration of thermal stress is developed for the calculation of PWAS impedance. Considering that the ISHM is a high-frequency method, the longitudinal vibration of the beam studied in this paper. One of the most widely used methods for the compensation of temperature in ISHM is cross-correlation (CC) method. This method uses frequency shift between baseline data and unknown data to compensate temperature effect on impedance signal. This method assumes that frequency shifts causing temperature variation in all modes of vibration are approximately the same. However, proposed thermal model show that shift of transverse mode was more than that of longitudinal mode. Therefore, CC method is not suitable for temperature compensation.

The corresponding author; Email:

In the present paper, in the first step, a thermal stress model for clamped-clamped Euler-Bernoulli beam is investigated. Then, the Rayleigh-Ritz method is used to discretize dynamic system. Finally, the electrical impedance of PWAS is calculated. In section 3 of this paper, SEM is to model PWAS on the beam with consideration of thermal stress. Then dynamic stiffness matrix calculated by SEM is used to compute the global spectral DOFs vector. This global DOFs vector was used to compute output impedance of PWAS. In the final section, results of SEM and Rayleigh-Ritz methods are compared showing that these two models could be used for the modeling of thermo-electro-mechanical in ISHM. Finally, the SEM result of the electrical impedance of PWAS is compared with 3D FEM.

2- Governing Equations

2- 1- Thermo-induced Beam Model

In Fig. 1 a clamped-clamped beam with PWAS is presented. The kinetic and strain energies of the beam can be calculated as follows using Euler-Bernoulli theory. Considering u_0, v_0 and w_0 of clamped-clamped beam displacements along x, y and z directions, respectively, we have:

$$u_0(x,t)=u(x,t)-zw'(x,t), v_0(x,t)=0 \\ w_0(x,t)=w(x,t) \tag{1}$$

The kinetic energy of the beam (T_b) can be calculated by

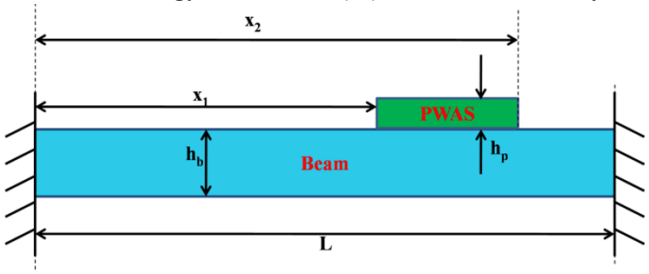

Fig. 1. Schematic of clamped-clamped beam with attached PWAS

$$T_b=\frac{1}{2}\int_0^L \overline{\rho_b A_b}\left[\dot{w}^2(x,t)+\dot{u}^2(x,t)\right]dx \tag{2}$$

For the sake of notational simplicity, the following notations for time and spatial derivatives have been used

$$\left\{\begin{matrix}\dot{\mathrm{P}}=\dfrac{\partial \mathrm{P}}{\partial t}\\ \mathrm{P}'=\dfrac{\partial \mathrm{P}}{\partial x}\end{matrix}\right\} \tag{3}$$

where

ρ_b is the density of beam with temperature dependency

A_b represents the cross-section area of the beam

L denotes the beam's length

Also, the superscript $\bar{\cdot}$ shows the dependency of material properties to temperature. To study the effect of PWAS, structure constants, and thermal stress variations on the structural response, the related strain results are used [16]:

$$\varepsilon_{xx}=u'(x,t)-zw''(x,t)+\frac{1}{2}w'^2(x,t) \\ \varepsilon_{xy}=\varepsilon_{yy}=\varepsilon_{zz}=\varepsilon_{yz}=\varepsilon_{xz}=0 \tag{4}$$

Because of the negligible difference between the linear and non-linear terms, we have the following equations for the strain energy (π_b) due to the generated strains:

$$\pi_b=\frac{1}{2}\int_V \sigma_{xx}\left(\varepsilon_{xx}-\alpha_b\Delta T\right)dV \tag{5}$$

$$\pi_b=\frac{1}{2}\int_0^L\left(\begin{matrix}\overline{E_b}Iw''(x,t)^2+\overline{E_b}A_bu'(x,t)^2\\ -\overline{E_b}A_b\alpha_b\Delta Tw'(x,t)^2+\alpha_b{}^2\Delta T^2\end{matrix}\right)dx \tag{6}$$

where

V is the volume of the beam; σ_{xx} is stress, and $\overline{E}_b$ is Young's modulus with temperature dependency.

I is the second moment of area. $\Delta T=T-T_0$ where T_0 is the reference temperature, and T is the temperature distribution through the beam, and the parameter α_b is the thermal expansion coefficient of the beam.

After applying Hamiltonian's principle, the transverse and longitudinal mode shape could be calculated from (5) and (6):

$$\left\{\begin{matrix}\overline{E_b}A_bu''=\overline{p}_bA_b\ddot{u}\\ \overline{E_b}Iw''''-\overline{E_b}A_b\alpha_b\Delta Tw''+\overline{p}_bA_b\ddot{w}=0\end{matrix}\right. \tag{7}$$

2- 2- Piezoelectric Actuator Model

The constitutive equation for the PWAS under thermal loading is given by[16]:

$$\sigma_1=E_p\left(e_1-\alpha_p\Delta T\right)-dE_3 \tag{8}$$

and

$$D_3=de_1+eE_3+p_3\Delta T \tag{9}$$

where

$$E_p=\frac{1}{\overline{S}_{11}^E} \tag{10}$$

$$d=\frac{\overline{d}_{31}}{\overline{S}_{11}^E} \tag{11}$$

$$e=\overline{\varepsilon}_{33}^T-\frac{\overline{d}_{31}^2}{\overline{S}_{11}^E} \tag{12}$$

ϵ_1 and σ_1 are mechanical strain and stress, respectively. E_3 and D_3 are the electrical field and electrical displacement, respectively. In addition, $\overline{S}^E_{11}$ is the mechanical compliance of the material measured at zero electric field and varies with temperature. $\overline{\varepsilon}^T_{33}$ represents the dielectric permittivity measured at zero mechanical stress and varies with temperature.d and e are direct and converse piezoelectric effect matrixes and varies with temperature. Consider a piezoelectric wafer with length L_p, width b_p, and thickness h_p, undergoing piezoelectric expansion induced by the thickness

polarization electric field E_3 as shown in Fig. 2. The kinetic energy (T_p) and strain energy (π_p) of PWAS, which is assumed to have a beam shape, can be obtained by:

$$T_p = \frac{1}{2}\int_{x_1}^{x_2} \overline{\rho}_p A_p \left[\dot{w}^2(x,t) + \dot{u}^2(x,t) \right] dx \tag{13}$$

$$\pi_p = \frac{1}{2}\int_{V_p} (\sigma_1 (e_1 - \alpha_p \Delta T) - D_3 E_3) dV_p \tag{14}$$

where
$\overline{\rho}_p$, A_p and V_p are density, area, and volume of PWAS, respectively.

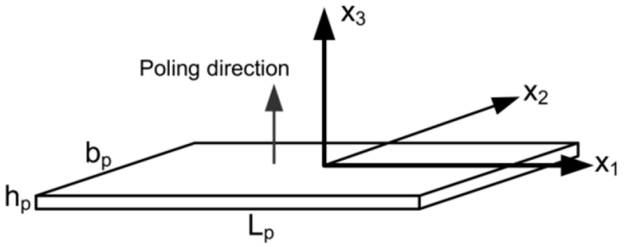

Fig. 2. Schematic of PWAS with a polarization direction

As shown in Fig. 1, x_1 is the distance of PWAS of the first edge from the origin and x_2 is the distance of PWAS of the last edge from the origin. Also, α_p is the thermal expansion coefficient of PWAS. Using (8), (9), and (14) can be rewritten as:

$$\pi_p = \frac{1}{2}\int_{x_1}^{x_2}\int_0^{b_p}\int_{\frac{h}{2}}^{\frac{h}{2}+h_p} \begin{pmatrix} (E_p (e_1 - \alpha_p \Delta T)^2 \\ -2de_1 E_3 \\ -eE_3{}^2 - p_3 \Delta T E_3) \end{pmatrix} dx\,dy\,dz \tag{15}$$

where e_1 is PWAS strain. Replacing $e_1 = u'(x,t) - zw''(x,t) + \frac{1}{2}w'^2(x,t)$ in (15), we have

$$\pi_p = \frac{1}{2}\int_{x_1}^{x_2} \begin{pmatrix} E_p A_p u'^2 + I_1 w''^2 - \\ E_p A_p \alpha_p \Delta T w'^2 - I_2 E_3 w' - \\ I_3 E_3{}^2 - p_3 \Delta T E_3 A_p - \\ 2\alpha_p \Delta T E_p A_p u' - \\ I_4 u' w'' + I_4 w'' - 2dE_3 u' \end{pmatrix} dx \tag{16}$$

with

$$I_1 = E_p b_p \frac{z^3}{3}\Big|_{\frac{h}{2}}^{\frac{h}{2}+h_p} \tag{17}$$

$$I_2 = db_p z^2 \Big|_{\frac{h}{2}}^{\frac{h}{2}+h_p} \tag{18}$$

$$I_3 = eb_p h_p \tag{19}$$

$$I_4 = 2E_p b \alpha_p \Delta T z^2 \Big|_{\frac{h}{2}}^{\frac{h}{2}+h_p} \tag{20}$$

2- 3- Coupling of Beam and Piezoelectric Actuator Models

After modeling kinetic and strain energies of the beam and PWAS, these energies must be used to model the coupling of the beam and PWAS effect. Thus, the kinetic energy (T) and the strain energy (π) of the beam and PWAS are

$$T = T_p + T_b \tag{21}$$

$$\pi = \pi_p + \pi_b \tag{22}$$

For the system discretization, Rayleigh-Ritz method is applied:

$$\begin{cases} w(x,t) = \sum_{i=1}^{n} \varphi_i(x) q_i(t) \\ u(x,t) = \sum_{i=1}^{n} \psi_i(x) p_i(t) \end{cases} \tag{23}$$

where $\varphi_i(x)$ and $\psi_i(x)$ are i-th transverse and longitudinal modal shape, respectively, which must satisfy boundary conditions. $q_i(t)$ and $p_i(t)$ are i-th transverse and longitudinal modal function, respectively. Using (21), (22) and (23) we have:

$$\begin{aligned} T = & \sum_{i=1}^{n}\sum_{j=1}^{n} \begin{pmatrix} \frac{1}{2}\int_{x_1}^{x_2} \overline{\rho}_p A_p \varphi_i(x)\varphi_j(x)\dot{q}_i(t)\dot{q}_j(t)dx \\ +\frac{1}{2}\int_0^L \overline{\rho_b} A_b \varphi_i(x)\varphi_j(x)\dot{q}_i(t)\dot{q}_j(t)dx \end{pmatrix} \\ & + \sum_{l=1}^{n}\sum_{k=1}^{n} \begin{pmatrix} \frac{1}{2}\int_{x_1}^{x_2} \overline{\rho}_p A_p \psi_l(x)\psi_k(x)\dot{p}_l(t)\dot{p}_k(t)dx \\ +\frac{1}{2}\int_0^L \overline{\rho_b} A_b \psi_l(x)\psi_k(x)\dot{p}_l(t)\dot{p}_k(t)dx \end{pmatrix} \end{aligned} \tag{24}$$

and

$$\begin{aligned} \pi = & \sum_{i=1}^{n}\sum_{j=1}^{n}\frac{1}{2}\int_0^L \begin{pmatrix} \overline{E}_b I \varphi_i''(x)\varphi_j''(x) - \\ \overline{E}_b A_b \alpha_b \Delta T \varphi_i'(x)\varphi_j'(x) \end{pmatrix} dx q_i(t) q_j(t) \\ & + \frac{1}{2}\int_{x_1}^{x_2} \begin{pmatrix} I_1 \varphi_i''(x)\varphi_j''(x) - \\ E_p A_p \alpha_p \Delta T \varphi_i'(x)\varphi_j'(x) \end{pmatrix} dx q_i(t) q_j(t) + \\ & \sum_{l=1}^{n}\sum_{k=1}^{n}\frac{1}{2}\int_{x_1}^{x_2} E_p A_p \psi_l'(x)\psi_k'(x) dx p_l(t) p_k(t) \\ & + \int_0^L \overline{E_b} A_b \psi_l'(x)\psi_k'(x) dx p_l(t) p_k(t) \\ & + \sum_{i=1}^{n}\frac{1}{2}\int_{x_1}^{x_2} -I_2 \varphi_i'(x) dx q_i(t) E_3) \\ & + \sum_{l=1}^{n}\frac{1}{2}\int_{x_1}^{x_2} -2dE_3 \psi_l'(x) dx p_l(t) E_3) + \\ & \sum_{i=1}^{n}\sum_{k=1}^{n}\frac{1}{2}\int_{x_1}^{x_2} -I_4 \varphi_i''(x)\psi_l'(x) dx q_i(t) p_l(t) E_3 + \\ & \sum_{i=1}^{n}\frac{1}{2}\int_{x_1}^{x_2} -I_4 \varphi_i''(x) dx q_i(t) + \\ & \sum_{l=1}^{n}\frac{1}{2}\int_{x_1}^{x_2} (-2\alpha_p \Delta T E_p A_p \psi_l'(x) p_l(t)) dx \\ & - I_3 L_p A_p E_3{}^2 - p_3 \Delta T E_3 A_p L_p \end{aligned} \tag{25}$$

Lagrange's equations without external load are

$$\frac{d}{dt}\left(\frac{\partial T}{\partial \dot{r}_j}\right)+\frac{\partial \pi}{\partial r_j}=0 \tag{25}$$

where r_j are variables of the strain and kinetic energies. Considering $r_j=q_i,p_l$, the results are as follows:

$$\begin{aligned}
&\sum_{j=1}^{n}\int_{x_1}^{x_2}\overline{\rho}_p A_p \varphi_i(x)\varphi_j(x)dx\,\ddot{q}_j(t)+\\
&\sum_{j=1}^{n}\int_{0}^{L}\overline{\rho_b} A_b \varphi_i(x)\varphi_j(x)dx\,\ddot{q}_j(t)+\\
&\sum_{j=1}^{n}\frac{1}{2}\int_{0}^{L}\begin{pmatrix}\overline{E}_b I\varphi_i''(x)\varphi_j''(x)-\\ \overline{E}_b A_b\alpha_b\Delta T\,\varphi_i'(x)\varphi_j'(x)\end{pmatrix}dx q_j(t)+\\
&\frac{1}{2}\int_{x_1}^{x_2}\begin{pmatrix}I_1\varphi_i''(x)\varphi_j''(x)-\\ E_p A_p\alpha_p\Delta T\,\varphi_i'(x)\varphi_j'(x)\end{pmatrix}dx q_j(t)+\\
&+\frac{1}{2}\int_{x_1}^{x_2}-I_2\varphi_i'(x)dxE_3+\\
&\sum_{l=1}^{n}\frac{1}{2}\int_{x_1}^{x_2}-I_4\varphi_i''(x)\psi_l'(x)dx p_l(t)+\\
&\frac{1}{2}\int_{x_1}^{x_2}-I_4\varphi_i''(x)dx=0
\end{aligned} \tag{26}$$

$$\begin{aligned}
&\sum_{l=1}^{n}\begin{pmatrix}\frac{1}{2}\int_{x_1}^{x_2}\overline{\rho}_p A_p\psi_l(x)\psi_k(x)\ddot{p}_l(t)dx+\\ \frac{1}{2}\int_{0}^{L}\overline{\rho}_b A_b\psi_l(x)\psi_k(x)\ddot{p}_l(t)dx\end{pmatrix}\\
&\sum_{l=1}^{n}\frac{1}{2}\int_{x_1}^{x_2}E_p A_p\psi_l'(x)\psi_k'(x)dx p_l(t)+\\
&\int_{0}^{L}\overline{E_b}A_b\psi_l'(x)\psi_k'(x)dx p_l(t)\\
&+\frac{1}{2}\int_{x_1}^{x_2}-2dE_3\psi_l'(x)dxE_3)+\\
&\sum_{i=1}^{n}\frac{1}{2}\int_{x_1}^{x_2}-I_4\varphi_i''(x)\psi_l'(x)dx q_i(t)\\
&+\sum_{l=1}^{n}\frac{1}{2}\int_{x_1}^{x_2}(-2\alpha_p\Delta TE_p A_p\psi_l'(x))dx=0
\end{aligned} \tag{27}$$

Two terms $\int_{x_1}^{x_2}(-2\alpha_p\Delta TE_p A_p\psi_l'(x))dx$ and $\int_{x_1}^{x_2}I_4\varphi_i''(x)dx$ are constant force and moment, respectively, and behave similarly to DC signals. DC signals do not affect impedance, thus these terms can be ignored in the calculation of impedance. Hence, (27) and (28) can be rewritten as follows:

$$M\,\ddot{qp}(t)+Kqp(t)=NE_3 \tag{28}$$

where M and K are the mass and stiffness matrixes of the system, respectively, and N is the force-moment vector created by PWAS actuator. For M and K, we have:

$$M=\begin{bmatrix}M_{buu}+M_{puu} & 0\\ 0 & M_{bww}+M_{pww}\end{bmatrix} \tag{29}$$

$$K=\begin{bmatrix}K_{buu}+K_{puu} & K_{buw}+K_{puw}\\ K_{bwu}+K_{pwu} & K_{bww}+K_{pww}\end{bmatrix} \tag{30}$$

$$N=\begin{bmatrix}N_{uu}\\ N_{ww}\end{bmatrix} \tag{31}$$

where M_{buu} and M_{bww} are the longitudinal and the transverse mass matrixes of the beam, respectively. M_{puu} and M_{pww} represent the longitudinal and the transverse mass matrixes of PWAS, respectively. K_{buu} and K_{bww} are the longitudinal and transverse stiffness matrixes of the beam, respectively. K_{puu} and K_{pww} denote the longitudinal and the transverse stiffness matrixes of PWAS. N_{uu} is the force vector created by PWAS actuator, and N_{ww} is the moment vector created by PWAS actuator. These parameters are given by:

$$M_{bww}=\int_{0}^{L}\overline{\rho_b}A_b\varphi_i(x)\varphi_j(x)dx \tag{32}$$

$$M_{pww}=\int_{x_1}^{x_2}\overline{\rho}_p A_p\varphi_i(x)\varphi_j(x)dx \tag{33}$$

$$M_{buu}=\int_{0}^{L}\overline{\rho_b}A_b\psi_l(x)\psi_k(x)dx \tag{34}$$

$$M_{puu}=\int_{x_1}^{x_2}\overline{\rho}_p A_p\psi_l(x)\psi_k(x)dx \tag{35}$$

$$K_{bww}=\int_{0}^{L}\begin{pmatrix}\overline{E}_b I\varphi_i''(x)\varphi_j''(x)-\\ \overline{E}_b A_b\alpha_b\Delta T\,\varphi_i'(x)\varphi_j'(x)\end{pmatrix}dx \tag{36}$$

$$K_{pww}=\frac{1}{2}\int_{x_1}^{x_2}\begin{pmatrix}I_1\varphi_i''(x)\varphi_j''(x)-\\ E_p A_p\alpha_p\Delta T\,\varphi_i'(x)\varphi_j'(x)\end{pmatrix}dx \tag{37}$$

$$K_{buu}=\int_{0}^{L}\overline{E_b}A_b\psi_l'(x)\psi_k'(x)dx \tag{38}$$

$$K_{puu}=\int_{x_1}^{x_2}E_p A_p\psi_l'(x)\psi_k'(x)dx \tag{39}$$

$$K_{buw}=K_{bwu}=\int_{x_1}^{x_2}-I_4\varphi_i''(x)\psi_l'(x)dx \tag{40}$$

$$N_{ww}=\int_{x_1}^{x_2}I_2\varphi_i'(x)dxE_3 \tag{41}$$

$$N_{uu}=\int_{x_1}^{x_2}-2dE_3\psi_l'(x)dx \tag{42}$$

Let qp(t), ψ(x) and φ(x) be the functions and shape model vectors defined as follow:

$$qp(t)=[p_1 \quad \dots \quad p_n \quad q_1 \quad \dots \quad q_n]^T \tag{43}$$

$$\psi(x)=[\psi_1(x) \quad \dots \quad \psi_n(x) \quad 0 \quad \dots \quad 0]^T \tag{44}$$

$$\varphi(x)=[0 \quad \dots \quad 0 \quad \varphi_1(x) \quad \dots \quad \varphi_n(x)]^T \tag{45}$$

The transform qp(t)=Tg(t) is applied to (29) where g(t) is the generalized coordinates of the system and T is the modal matrix built up by eigenvectors of the system. By this transformation, (29) becomes:

$$MT\ \ddot{g}(t)+KT\ \ g(t)=NE_3 \tag{46}$$

Pre-multiplying (46) by T^T, we have

$$T^T MT\ \ddot{g}(t)+T^T KT\ \ g(t)=T^T NE_3 \tag{47}$$

This can be rewritten as:

$$M^*\ddot{g}(t)+K^*g(t)=T^T NE_3 \tag{48}$$

where matrices M^* and K^* attained from $M^*=T^TMT$ and $K^*=T^TKT$ and are called the generalized mass and the generalized stiffness matrices, respectively.

$$M^*\ddot{g}(t)+K^*g(t)=T^T NE_3 \tag{49}$$

If the PWAS is thin enough, then the generated electrical field is equal to:

$$E_3=\frac{V_3}{h_p} \tag{50}$$

$V_3(t)=V_0e^{i\omega t}$ is a harmonic voltage between the top and bottom surfaces electrodes. From (50) and (51), it is achieved that

$$M^*\ddot{g}(t)+K^*g(t)=N^*V_3 \tag{51}$$

with $N^*=\dfrac{(T^TN)}{h_p}$

Because, the voltage excitation is harmonic, the generalized coordinates are in the form of $g(t)=g_0e^{i\omega t}$.
Introducing $g(t)=g_0e^{i\omega t}$ to (52), we obtain:

$$g_0=(-M^*\omega^2+K^*)^{-1}N^*V_0 \tag{52}$$

Also, the modal function vector can be calculated as:

$$qp_0=T(-M^*\omega^2+K^*)^{-1}N^*V_0 \tag{53}$$

2- 4- Electrical Response of PWAS

Recalling (9) as $D_3 = d\in_1 + eE_3 + p_3\Delta T$, because $p_3\Delta T$ is constant, this term was not considered in impedance calculation.

$$D_3=d\ \in_1+eE_3 \tag{54}$$

Integration of D_3 over the electrodes area A_p yields the total charge Q(t):

$$Q(t)=\int_{A_p}D_3dA_p \tag{55}$$

Inserting (9) in (56) results in:

$$Q(t)=\int_{x_1}^{x_2}\int_0^{b_p}(d\ \in_1+eE_3)dxdy \tag{56}$$

Substitute $\in_1$ for (4) and set $z=\dfrac{h_b}{2}$, we have:

$$Q(t)=-db_p\left(\frac{h_b}{2}\right)w'(x,t)\Big|_{x_1}^{x_2}+db_pu(x,t)\Big|_{x_1}^{x_2} +eE_3b_pL_p \tag{57}$$

Using Rayleigh Ritz method, we obtain:

$$Q(t)=\left(-db_p\left(\frac{h_b}{2}\right)\varphi'(x)\Big|_{x_1}^{x_2}+db_p\psi(x)\Big|_{x_1}^{x_2}\right) qp(t)+\frac{eV_3b_pL_p}{h_p} \tag{58}$$

Introducing (54) into (58), we get:

$$Q(t)=\left(-db_p\left(\frac{h_b}{2}\right)\varphi'(x)\Big|_{x_1}^{x_2}+db_p\psi(x)\Big|_{x_1}^{x_2}\right) \times\left(T(-M^*\omega^2+C^*i\omega+K^*)^{-1}N^*+\frac{eb_pL_p}{h_p}\right)V_0e^{i\omega t} \tag{59}$$

The time derivative of the electric charge is the electric current, i.e.

$$I(t)=\dot{Q}(t)=i\omega Q(t) \tag{60}$$

Hence,

$$I(t)=i\omega\left(-db_p\left(\frac{h_b}{2}\right)\varphi'(x)\Big|_{x_1}^{x_2}+db_p\psi(x)\Big|_{x_1}^{x_2}\right) \times T(-M^*\omega^2+C^*i\omega+K^*)^{-1}N^*+\frac{eb_pL_p}{h_p}\Big)V_0e^{i\omega t} \tag{61}$$

The impedance, Z, which is defined as the ratio of the voltage to current, can be calculated by:

$$Z(i\omega)=\frac{V_3(t)}{I(t)}=\left(\begin{array}{l} i\omega\left(-db_p\left(\frac{h_b}{2}\right)\varphi'(x)\Big|_{x_1}^{x_2}+db_p\psi(x)\Big|_{x_1}^{x_2}\right) \\ \times T(-M^*\omega^2+C^*i\omega+K^*)^{-1}N^* \\ +\frac{eb_pL_p}{h_p}) \end{array}\right)^{-1} \tag{62}$$

3- Spectral Element Method (SEM)

Lee [15] applied SEM to model a dynamic system for a beam with PWAS [15]. In this section, SEM was used to calculate PWAS. But, a little change must be made in Lee's equation. First, it is assumed that viscous damping coefficient is zero ($c_b=0, c_p=0$) in Lee's equation, in which c_b and c_p are viscous damping coefficients of the beam and PWAS, respectively. Therefore only the structural damping of the base beam and

PWAS is considered using the complex modulus [9].
Then, the frequency-domain expression of the equations of motion is in [15]:

$$\begin{cases} EIW'''' - \omega^2 \rho A W = \omega^2 \alpha U' + \\ \beta U''' - \omega^2 \gamma W'' + F W'' \\ EA\, U'' + \omega^2 \rho A\, U = \omega^2 \alpha W' + \beta W''' \end{cases} \tag{63}$$

where

$$EA = E_b A_b + E_p A_p, \qquad EI = E_b I_b + E_p I_p$$
$$\rho A = \rho_b A_b + \rho_p A_p, \qquad \alpha = \frac{1}{2}\rho_p A_p (h_b + h_p) \tag{64}$$
$$\beta = \frac{1}{2} E_p A_p (h_b + h_p), \quad \gamma = 4\rho_p A_p (h_b + h_p)^2$$

Despite the reference [15] which considered f as a constant axial tensile force, this work introduce f as an applied thermal stress to the beam The boundary conditions are as follow [15]:

$$\begin{aligned} &Q(0) = -Q_1 - F W'(0) \quad or \quad W(0) = W_1 \\ &M(0) = -M_1 \quad or \quad W'(0) = \theta_1 \\ &N(0) = -N_1 \quad or \quad U(0) = U_1 \\ &Q(L) = -Q_2 - F W'(L) \quad or \quad W(L) = W_2 \\ &M(L) = -M_2 \quad or \quad W'(L) = \theta_2 \\ &N(L) = -N_2 \quad or \quad U(L) = U_2 \end{aligned} \tag{65}$$

The force-displacement relationships give [15]:

$$\begin{aligned} &Q(x) = -EIW''' + \omega^2 \alpha U + \beta U'' - \omega^2 \gamma W' \\ &M(x) = EIW''' - \beta U' \\ &N(x) = EA\, U' - \beta W'' \end{aligned} \tag{66}$$

The general solutions of (64) are assumed to be

$$W(x;\omega) = r_w A e^{-ikx}, \quad U(x;\omega) = r_u A e^{-ikx} \tag{67}$$

Thus, the eigenvalue problem is given by

$$\begin{bmatrix} X_{11} & X_{12} \\ X_{12} & X_{22} \end{bmatrix} \begin{bmatrix} r_w \\ r_u \end{bmatrix} = \begin{bmatrix} 0 \\ 0 \end{bmatrix} \tag{68}$$

where

$$\begin{cases} X_{11} = EIk^4 - \rho A \omega^2 - \omega^2 \gamma k^2 + Fk^2 \\ X_{22} = -k^2 EA + \rho A \omega^2 \\ X_{12} = i\omega^2 k \alpha - ik^3 \beta \end{cases} \tag{69}$$

Because c_b=0, c_c=0, if α=β=0, (an element without PWAS) or $\frac{EA}{\rho A} \approx \frac{\beta}{\alpha}$, then $X_{22} \approx -X_{12}$ and the determinant of the matrix (68) will be $X_{22}(X_{11}+X_{12})=0$. It in turn means $X_{22}=0$, $(X_{11}+X_{12})=0$

Therefore, the transverse and the longitudinal vibrations will be decoupled and matrix H(ω), introduced in [15], will be singular. Thus, the general solutions of (55) can be written as:

$$\begin{aligned} W(x;\omega) &= \sum_{j=1}^{6} r_w A_j e^{-ik_j x} = e(x;\omega) R_w a \\ U(x;\omega) &= \sum_{j=1}^{6} r_u A_j e^{-ik_j x} = e(x;\omega) R_u a \end{aligned} \tag{70}$$

where k_1, k_4 are the solutions of $X_{22}=0$, and k_2, k_3, k_5, k_6 are the solutions of $(X_{11}+X_{12})=0$ Also,

$$e(x;\omega) = [e^{-ik_1 x} \;\; e^{-ik_2 x} \;\; e^{-ik_3 x} \;\; e^{-ik_4 x} \;\; e^{-ik_5 x} \;\; e^{-ik_6 x}] \tag{71}$$

where

$$a = \{A_1 \;\; A_2 \;\; A_3 \;\; A_4 \;\; A_5 \;\; A_6\} \tag{72}$$

and

$$\begin{aligned} R_w &= diag(0,1,1,0,1,1), \\ R_u &= diag(1,0,0,1,0,0) \end{aligned} \tag{73}$$

The spectral nodal degrees-of-freedom (DOFs) of the beam is shown in Fig. 3.

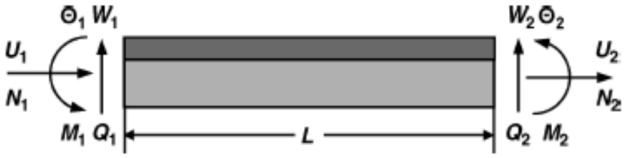

Fig. 3. Spectral element of beam with PWAS [15]

Let the spectral nodal DOFs vector be

$$\begin{aligned} d &= \{U_1 \;\; W_1 \;\; \theta_1 \;\; U_2 \;\; W_2 \;\; \theta_2\}^T = \\ &= \{U(0) \;\; W(0) \;\; \theta(0) \;\; U(L) \;\; W(L) \;\; \theta(L)\}^T \end{aligned} \tag{74}$$

Applying (71) to the spectral nodal DOFs defined by (75), we obtain

$$d = H(\omega) a \tag{75}$$

where H(ω) is the following 6×6 matrix:

$$H(\omega) = \begin{bmatrix} e(0;\omega) R_u \\ e(0;\omega) R_w \\ \dfrac{de(0;\omega)}{dx} R_w \\ e(L;\omega) R_u \\ e(L;\omega) R_w \\ \dfrac{de(L;\omega)}{dx} R_w \end{bmatrix} \tag{76}$$

The dynamic shape functions are defined by

$$\begin{aligned} W(x;\omega) &= e(x;\omega) R_w H^{-1}(\omega) d, \\ U(x;\omega) &= e(x;\omega) R_u H^{-1}(\omega) d \end{aligned} \tag{77}$$

According to Fig. 3, the spectral nodal moment and force are given by:

$$f_c = \{N_1\ Q_1\ M_1\ N_2\ Q_2\ M_2\}^T = \\ = \{-N(0) - Q(0) - \\ FW'(0)\ M(0)\ N(L)\ Q(L) \\ + FW'(L)\ M(L)\}^T \quad (78)$$

If the spectral nodal DOFs include PWAS, then $f(\omega) = f_c^{PWAS} V(\omega) + f_c^{mesh}$, else $f(\omega) = f_c^{mesh}$, else where

$$f_c^{mesh} = \{N_1\ Q_1\ M_1\ N_2\ Q_2\ M_2\}^T = \\ = \{-N(0) - Q(0) - \\ FW'(0)\ M(0)\ N(L)\ Q(L) + \\ FW'(L)\ M(L)\}^T \quad (79)$$

and

$$f_c^{PWAS} = \{-N_p\ \ 0\ M_p\ \ N_p\ \ 0\ \ -M_p\}^T \quad (80)$$

$$M_p = \frac{1}{2} b (h_b + h_p) d_{31} E_p, \quad N_p = b d_{31} E_p, \quad (81)$$

For the thermal stress induced in structure and PWAS, if spectral nodal DOFs contain PWAS, then $F = -(E_p A_p \alpha_p + E_b A_b \alpha_b)\Delta T$, otherwise $F = -(E_b A_b \alpha_b)\Delta T$. The other equations would be similar to those given in [15]. If $\frac{EA}{\rho A} \neq \frac{\beta}{\alpha}$, the equations introduced in [15] are valid. The spectral elements represented by Lee [15] can be assembled to form a global system equation as

$$S_g(\omega) d_g = f_g(\omega) \quad (82)$$

where $S_g(\omega)$ is the global dynamic stiffness matrix, d_g is the global spectral DOFs vector, and $f_g(\omega)$ is the global spectral nodal forces vector. After finding d_g, the electrical charge can be calculated from (9)

$$Q(\omega) = \begin{pmatrix} -db_p \left(\frac{h}{2}\right) W'(x;\omega)\Big|_{x_1}^{x_2} + \\ db_p U(x;\omega)\Big|_{x_1}^{x_2} + \frac{eb_p L_p}{h_p} \end{pmatrix} V_3(\omega) \quad (83)$$

PWAS impedance is obtained from:

$$Z(i\omega) = \left(i\omega \begin{pmatrix} -db_p \left(\frac{h}{2}\right) W'(x;\omega)\Big|_{x_1}^{x_2} \\ + db_p U(x;\omega)\Big|_{x_1}^{x_2} + eb_p L_p \end{pmatrix} \right)^{-1} \quad (84)$$

4- Numerical Solution And Discussion

4- 1- Ambient Temperature

Several numerical simulations were used to predict PWAS impedance during structural identification. Structural vibration analysis theory and SEM have been used for numerical simulation. Because in this simulation $\frac{EA}{\rho A} \approx \frac{\beta}{\alpha}$ for SEM, (71)-(74) must be used to model PWAS impedance. The numerical results have been calculated for the transverse and longitudinal frequencies and mode shapes of the beam. These frequencies are almost identical with the basic beam natural frequencies as predicted by vibration analysis. Tables 1 and 2 show Aluminum beam and PWAS constants, respectively, at 25°C. Table 3 represents the Rayleigh-Ritz and SEM results related to the first seven natural frequencies for the temperature 25°C. These theoretical results have been calculated by beam vibration theory A) beam containing PWAS, B) without PWAS. SEM (N) show N equivalent dynamic point forces for the analysis results.

Table 3 shows the differences between Rayleigh-Ritz and SEM results (see column 6 in which Δ% represents the percentage of error) and between beam vibration theory and SEM (see column 7 in which Δ% denotes the percentage of the related error). The natural frequencies obtained by Rayleigh-Ritz model are in good agreement with those of calculated by SEM.

Table 1. geometrical and material properties of aluminum beam

Property	Symbol	Value
Length	L_b	15cm
Width	b	1cm
Thickness	h_b	5mm
Density	ρ_b	2699.99 kg/m^3
Complex Young's Module	E_b	68.998(1+10^{-5}i)Gpa

Table 2. geometrical and material properties of pwas psi 5H4E

Property	symbol	value
Length	L_p	1cm
Width	b_p	1cm
Thickness	h_p	0.267mm
Density	ρ_p	7749.985 kg/m^3
Compliance, in plane	S^E_{11}	1.64×10^{-11} pa^{-1}
In-plane induced-strain coefficient	d_{31}	–320.026×10^{-12} m/V
Dielectric Constant	ε^T_{33}	ε^T_{33}=3800 ε_0
Dielectric Constant in the air	ε_0	8.85×10^{-12} F/m
distance of PWAS first edge from the origin	x_1	12cm
distance of PWAS end edge from the origin	x_2	$x_2 = x_1 + L_p$

Table 3. natural frequencies of system obtained by sem (5) and rayleigh-ritz method (a: with pwas, b: without pwas)

	Vibration mode	A) Rayleigh-Ritz with PWAS (kHz)	B) Theo-without PWAS (kHz)	SEM(5) (kHz)	Δ% with PWAS	Δ% without PWAS
1	Transverse	6.2763	6.2643	6.270	0.1005	-0.0909
2	Transverse	10.4	10.3552	10.385	0.1444	-0.2870
3	Transverse	15.536	15.4688	15.515	0.1354	-0.2978
4	longitudinal	16.99	16.9073	16.973	0.1002	-0.3871
5	Transverse	21.685	21.6053	21.636	0.2265	-0.1419
6	Transverse	28.861	28.7644	28.769	0.3198	-0.0160
7	longitudinal	33.723	33.8147	33.710	0.0386	0.3106

Table 4. value of frequency shift obtained by sem (5) results (25°c, 50°c)

	Vibration modes	25°C SEM(5) (kHz)	50°C SEM(5) (kHz)	50°C SEM(5) varying Temp Material (kHz)	difference column 2, 3 (Hz)	difference column 2, 4 (Hz)
1	Transverse	6.270	6.1388	6.0913	-131.2	-178.7
2	Transverse	10.385	10.248	10.169	-137	-216
3	Transverse	15.515	15.374	15255	-141	-260
4	longitudinal	16.973	16.973	16.841	0	-132
5	Transverse	21.636	21.491	21.325	-145	-311
6	Transverse	28.769	28.623	28.401	-146	-368
7	longitudinal	33.710	33.710	33.449	0	-261

Table 5. value of frequency obtained by sem (5) and fem(30889) results (25°c, 50°c)

	Vibration modes	25°C SEM(5) (kHz)	25°C FEM(30889) (kHz)	Δ% in 25°C	50°C SEM(5) (kHz)	50°C FEM(30889) (kHz)	Δ% in 25°C
1	Transverse	6.270	6.430	2.4883	6.1388	6.310	0.6339
2	Transverse	10.385	10.47	0.8118	10.248	10.28	-1.0214
3	Transverse	15.515	15.35	1.0749	15.374	15.12	-2.6124
4	longitudinal	16.973	18.02	5.8102	16.973	17.97	5.5481
5	Transverse	21.636	20.96	3.2252	21.491	20.81	-3.9692
6	Transverse	28.769	27.24	5.6131	28.623	27.16	-5.9242
7	longitudinal	33.710	34.14	1.2595	33.710	33.87	0.4724

Fig. 4 shows the Rayleigh-Ritz and SEM results for the real part of PWAS impedance.

This figure represents that the Rayleigh-Ritz results are close to SEM results. Because SEM considers element modeling, it results in better data than that of obtained by Rayleigh-Ritz method. However, as can be seen in Table 3 and Fig. 4, the difference between two methods is very low.

4- 2- Varying Temperature

In this section, the effect of temperature variation, in the range of 25°C to 50°C, on the impedance signature of the PWAS sensor was investigated. For this propose, two conditions were considered. First, only the effect of thermal stress on beam was simulated. In the second study, the temperature variations of beam and PWAS materials were considered.

The constants of Aluminum and PWAS materials, which vary with temperature, were set according to [8]. Fig. 5 shows the real part of impedance of the beam in 25°C, 35°C, and 50°C for Rayleigh-Ritz method. Solid lines show the effect of sole thermal stress on the impedance of PWAS while the dashed line represents impedance variation when the two factors of thermal stress and temperature variation of beam and PWAS material are considered. This figure shows that the real part of PWAS impedance has been moved to left with the increase of temperature. Fig. 6 shows the same results for SEM. The numerical data was tabulated in Table 4.

According to Fig. 5, when only thermal stress has been considered in the model, longitudinal vibration mode has a zero shift between 25°C and 50°C (see Equation (7)). However, considering the two factors of thermal stress and temperature variation of beam and PWAS materials, a significant frequency shift observed.

Thus, for a good modeling on ISHM with the temperature effect, not only the thermal stress but also the beam and PWAS materials varying with the temperature should be considered.

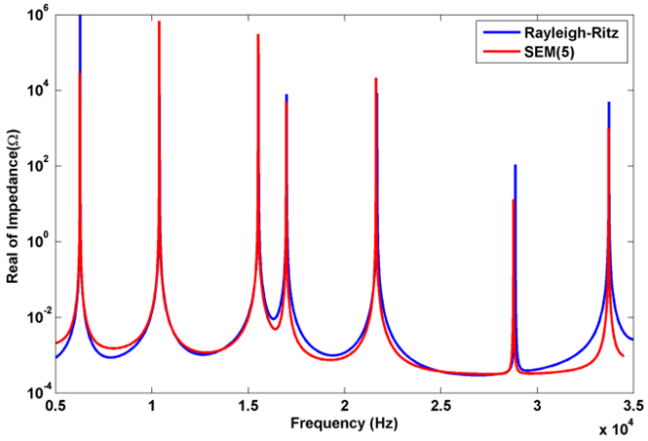

Fig. 4. Rayleigh-Ritz and SEM (5) results of real impedance of PWAS for the cantilever beam (25°C)

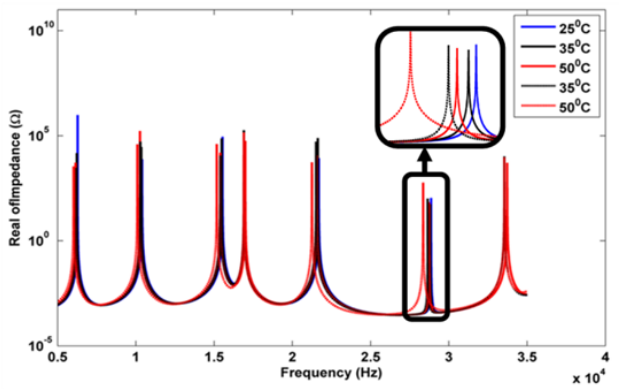

Fig. 5. Real impedance of PWAS obtained by Rayleigh-Ritz for different temperatures (25°C, 35°C and 50°C) Solid lines show only the thermal stress on the structure and dash line shows the two factors of thermal stress and temperature variation of beam and PWAS material.

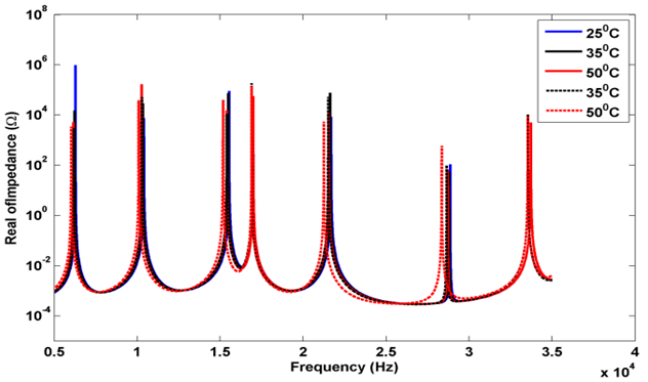

Fig. 6. PWAS real impedance obtained by SEM(5) for different temperatures (25°C, 35°C and 50°C) Solid lines show only thermal stress on the structure and dash line shows the two factors of thermal stress and temperature variation of beam and PWAS material.

The effect of sudden changes in temperature from 25°C to 50°C during the sampling rate for SEM (5) is demonstrated in Fig. 6. Depending on when these changes occur during sampling rate, it would be a great effect on the impedance. Therefore, CC method is not suitable for the compensation of temperature. Equations of the model considered with the thermal stress were solved numerically using commercial 3D FEM. A schematic of 3D FEM is shown in Fig. 7. The number

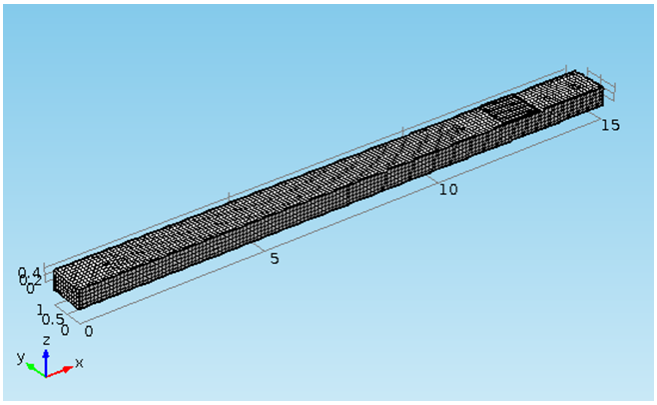

Fig. 7. 3D FEM for fully clamped beam in commercial software

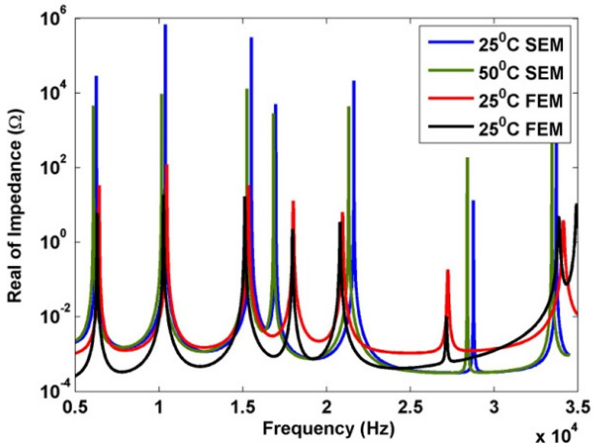

Fig. 8. PWAS real impedance obtained by SEM and FEM for different temperature (25°C and 50°C)

of degrees of freedom for 3D FEM is set 30889. Table 5 shows the natural frequencies obtained from SEM and 3D FEM for 25°C and 50°C. This table shows that natural frequencies of SEM (5) and 3D FEM (30889) are much closer to each other. SEM only uses 5 DOFs while FEM uses 30889 DOFs. The runtime is very high in FEM.

Fig. 8 shows the real part of impedance using SEM and 3D FEM versus frequency for the temperatures 25°C and 50°C. Results show a good agreement between SEM and 3D FEM.

5- Conclusion

In this paper, we studied the influence of thermal stress on the structural response in ISHM with the aim of obtaining a good theoretical model which reduces the need for doing costly and time-consuming experimental tests. For this propose, a coupling of PWAS and beam using Rayleigh-Ritz and SEM have been presented. This method does not apply equal moment and force because of using energy method. Also, we found out considering the effect of thermal stress with a temperature variation of PWAS material leads to a better modeling of temperature effects. Meanwhile, results show that thermal stress should be considered in order to compensate the temperature effects in ISHM. One of the most widely used methods to compensate temperature in ISHM is cross correlation (CC) method. This method uses frequency shift between baseline data and unknown data to compensate temperature effect on impedance signal. This method assumes that frequency shifts causing temperature variation, in all modes of vibration are approximately the

same. But using the proposed thermal model, it was shown that the transverse mode more shifts than the longitudinal mode. Thus, CC could not work very well in general cases for the compensation of temperature on impedance signals.

REFERENCES

[1] V. Giurgiutiu, C. Rogers, Electro-mechanical (E/M) impedance method for structural health monitoring and nondestructive evaluation, Structural Health Monitoring—Current Status and Perspective, (1997) 18-20.

[2] G. Park, H.H. Cudney, D.J. Inman, Feasibility of using impedance-based damage assessment for pipeline structures, Earthquake engineering & structural dynamics, 30(10) (2001) 1463-1474.

[3] S. Bhalla, A.S.K. Naidu, C.K. Soh, Influence of structure-actuator interactions and temperature on piezoelectric mechatronic signatures for NDE, in: Smart Materials, Structures, and Systems, International Society for Optics and Photonics, 2003, pp. 263-270.

[4] K.-Y. Koo, S. Park, J.-J. Lee, C.-B. Yun, Automated impedance-based structural health monitoring incorporating effective frequency shift for compensating temperature effects, Journal of Intelligent Material Systems and Structures, 20(4) (2009) 367-377.

[5] G. Park, K. Kabeya, H.H. Cudney, D.J. Inman, Impedance-based structural health monitoring for temperature varying applications, JSME International Journal Series A Solid Mechanics and Material Engineering, 42(2) (1999) 249-258.

[6] A. Bastani, H. Amindavar, M. Shamshirsaz, N. Sepehry, Identification of temperature variation and vibration disturbance in impedance-based structural health monitoring using piezoelectric sensor array method, Structural Health Monitoring, 11(3) (2012) 305-314.

[7] N. Sepehry, M. Shamshirsaz, F. Abdollahi, Temperature variation effect compensation in impedance-based structural health monitoring using neural networks, Journal of Intelligent Material Systems and Structures, 22(17) (2011) 1975-1982.

[8] N. Sepehry, M. Shamshirsaz, A. Bastani, Experimental and theoretical analysis in impedance-based structural health monitoring with varying temperature, Structural Health Monitoring, 10(6) (2011) 573-585.

[9] V. Giurgiutiu, Structural health monitoring: with piezoelectric wafer active sensors, Academic Press, 2007.

[10] A.N. Zagrai, V. Giurgiutiu, Electro-mechanical impedance method for crack detection in thin wall structures, in: 3rd Int. Workshop of Structural Health Monitoring, 2001, pp. 12-14.

[11] S. Bhalla, C.K. Soh, Electromechanical impedance modeling for adhesively bonded piezo-transducers, Journal of Intelligent Material Systems and Structures, 15(12) (2004) 955-972.

[12] D.M. Peairs, D.J. Inman, G. Park, Circuit analysis of impedance-based health monitoring of beams using spectral elements, Structural Health Monitoring, 6(1) (2007) 81-94.

[13] S. Bhalla, C.K. Soh, Structural health monitoring by piezo-impedance transducers. I: Modeling, Journal of Aerospace Engineering, 17(4) (2004) 154-165.

[14] W. Yan, W. Chen, C. Lim, J. Cai, Application of EMI technique for crack detection in continuous beams adhesively bonded with multiple piezoelectric patches, Mechanics of Advanced Materials and Structures, 15(1) (2008) 1-11.

[15] U. Lee, Spectral element method in structural dynamics, John Wiley & Sons, 2009.

[16] Y. Kiani, S. Taheri, M. Eslami, Thermal buckling of piezoelectric functionally graded material beams, Journal of Thermal Stresses, 34(8) (2011) 835-850.

Please cite this article using:

N. Sepehry, F. Bakhtiari-Nejad,M. Shamshirsaz, Thermo-Electro Mechanical Impedance based Structural Health Monitoring: Euler-Bernoulli Beam Modeling, *AUT J. Model. Simul., 49(2)(2017)143-152*.

DOI: 10.22060/miscj.2016.841